CONDENSED MATTER PHYSICS

The role of ultrafast magnon generation in the magnetization dynamics of rare-earth metals

B. Frietsch[1], A. Donges[2], R. Carley[1]*, M. Teichmann[1]*, J. Bowlan[1†], K. Döbrich[1], K. Carva[3,4], D. Legut[5], P. M. Oppeneer[1,3], U. Nowak[2], M. Weinelt[1‡]

Ultrafast demagnetization of rare-earth metals is distinct from that of 3d ferromagnets, as rare-earth magnetism is dominated by localized 4f electrons that cannot be directly excited by an optical laser pulse. Their demagnetization must involve excitation of magnons, driven either through exchange coupling between the 5d6s-itinerant and 4f-localized electrons or by coupling of 4f spins to lattice excitations. Here, we disentangle the ultrafast dynamics of 5d6s and 4f magnetic moments in terbium metal by time-resolved photoemission spectroscopy. We show that the demagnetization time of the Tb 4f magnetic moments of 400 fs is set by 4f spin–lattice coupling. This is experimentally evidenced by a comparison to ferromagnetic gadolinium and supported by orbital-resolved spin dynamics simulations. Our findings establish coupling of the 4f spins to the lattice via the orbital momentum as an essential mechanism driving magnetization dynamics via ultrafast magnon generation in technically relevant materials with strong magnetic anisotropy.

INTRODUCTION

Uncovering the nature of ultrafast spin phenomena under strongly nonequilibrium conditions is an intriguing fundamental research question at the frontier of condensed matter physics. Upon excitation of a material with a femtosecond optical pulse, the valence electronic system is pushed out of equilibrium within the laser pulse duration. During the time scale to establish subsequently thermal equilibrium among excited electrons, lattice, and spin systems of typically several picoseconds, the medium is in a transient and strongly nonequilibrium state. In this state, previously unknown phenomena occur, which cannot be observed in thermal equilibrium when simply heating the magnetic system (*1*–*4*). Fundamental magnetic properties such as the intra-atomic exchange interaction (*5*), exchange splitting (*6*), and spin mixing (*3*, *7*) manifest nonequilibrium behavior. In composite magnetic materials, the magnetic moments on distinct sublattices react differently (*2*) despite strong interatomic exchange J_{ij} constants that couple the magnetic moments on the different sublattices together. This distinct nonequilibrium behavior of constituting spin systems seems pivotal for all-optical magnetic switching where a single femtosecond laser pulse is sufficient to revert the magnetization of synthetic ferrimagnets (*8*–*10*). Therefore, it is essential to understand which are the decisive couplings between electrons, phonons, and spins that drive magnetization dynamics in the first few picoseconds after femtosecond laser excitation.

In their pioneering work, Beaurepaire *et al.* (*1*) not only established ultrafast demagnetization of nickel but also proposed that the coupling between electron and spin baths drives femtosecond magnetization dynamics while the lattice response lags behind. Notwithstanding, one of today's models of ultrafast demagnetization is based on spin-lattice coupling through Elliott-Yafet spin relaxation (*11*, *12*), in which angular momentum of hot valence electrons is transferred on a subpicosecond time scale to the cooler phonons, as claimed to have been observed recently (*13*). An alternative explanation is the superdiffusive spin transport (*14*), in which hot electrons transport angular momentum out of the excitation region.

A reversed process, exciting spins by hot phonons via spin-lattice coupling, must however become important when the spin subsystem, embedded in the underlying electronic system, is not excited by the optical pump pulse (*15*). This is in particular true for the correlated rare-earth metals, where optical excitation with 1.5-eV laser pulses heats the 5d6s valence electrons that carry only a small spin moment (~0.4 μ_B), while the more strongly bound, localized 4f levels, which carry most of the magnetic moment, remain unaffected (*6*). As sketched in Fig. 1 (A and B), there exist two distinct pathways in which excitation of the 4f spins can occur: via coupling to the excited 5d spin moment, involving the 5d-4f intra-atomic exchange J_{intra}, and/or via excitation of the lattice, expressed by the electron-phonon coupling G_{ep} and subsequent coupling of the 4f angular momentum to lattice motions (indicated by α_{4f}). In metals, heating of the crystal lattice sets in immediately upon optical excitation by scattering of hot electrons with phonons and completes roughly within 2 ps. The coupling of these lattice motions to the 4f spin S is mediated by the orbital momentum L, via spin-orbit coupling $\sim \xi \hat{L} \cdot \hat{S}$. In gadolinium, the coupling of the lattice to the spin moment is expected to be very weak ($L = 0$, $S = 7/2$, $J = L + S = 7/2$), but it is strong for Tb ($L = 3$, $S = 3$, $J = 6$), with J as the total angular momentum quantum number of the 4f shell (*15*–*17*). Earlier experiments by Vaterlaus *et al.* (*18*) suggest that spin-lattice coupling in gadolinium occurs on a rather slow time scale of 100 ± 80 ps. We note that in the ferromagnetic rare-earth metals, flipping a 4f spin would require several μ_B angular momentum transfer and several electron volts of excitation energy per atom. However, launching spin waves and phonons requires

[1]Fachbereich Physik, Freie Universität Berlin, Arnimallee 14, 14195 Berlin, Germany. [2]Fachbereich Physik, Universität Konstanz, 78457 Konstanz, Germany. [3]Department of Physics and Astronomy, Uppsala University, P. O. Box 516, S-75120 Uppsala, Sweden. [4]Charles University, Faculty of Mathematics and Physics, DCMP, Ke Karlovu 5, CZ-12116 Prague 2, Czech Republic. [5]IT4Innovations-Czech National Supercomputing Centre, VSB–Technical University Ostrava, 17. listopadu 2172/15, CZ-708 00 Ostrava, Czech Republic.
*Present address: European XFEL, Holzkoppel 4, 22869 Schenefeld, Germany.
†Present address: Los Alamos National Laboratory, Physical Chemistry and Applied Spectroscopy, Los Alamos, NM 87545, USA.
‡Corresponding author. Email: weinelt@physik.fu-berlin.de

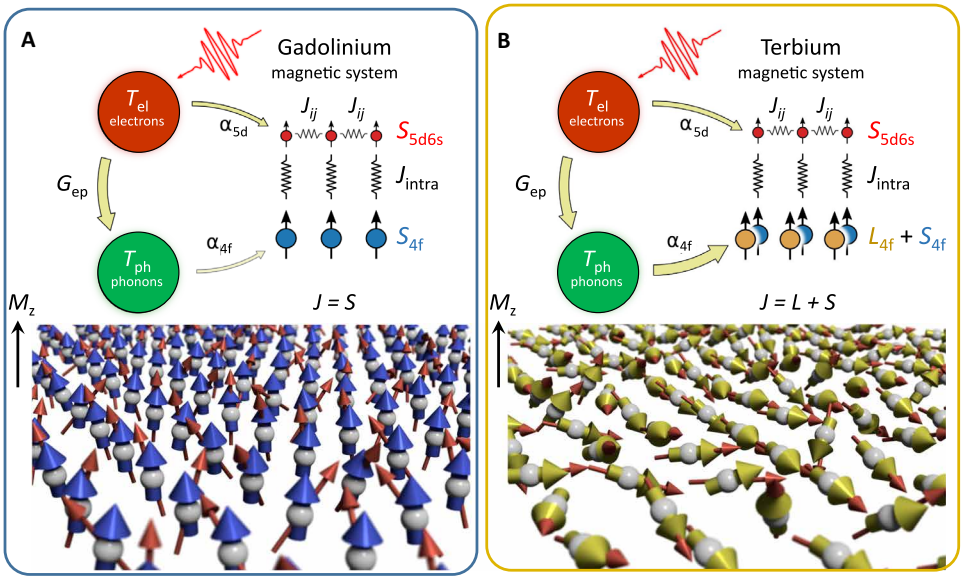

Fig. 1. Comparison of 5d6s and 4f spin dynamics in Gadolinium and Terbium. Upper panels: Orbital-resolved spin model. The yellow arrows represent the energy flow from the laser-excited electrons into the lattice (G_{ep}) and to the 5d and 4f spin systems. Note the different 4f spin–to–lattice couplings α_{4f} in (**A**) Tb ($J = L + S = 6$, $L = 3$) and (**B**) Gd ($J = S = 7/2$, $L = 0$). In contrast, inter- and intra-atomic exchange constants (J_{ij} and J_{intra}) are of comparable magnitude. Lower panels: Illustration of 5d6s and 4f spin dynamics about 1 ps after laser excitation. While in (B), the 4f spins (yellow arrows) are strongly excited by lattice motions and tilted with respect to M_z, in (A), they remain cold and aligned along the magnetization direction M_z. The 5d6s spins (red arrows) are additionally coupled to the optically excited valence electrons α_{5d} and thus quiver around the 4f moments.

comparable energies of few millielectron volts (*19*). Tb even shows an avoided crossing of phonon and magnon (=spin-wave) branches indicative of strong phonon-magnon coupling (*19*).

Figure 1 illustrates the different couplings for the Gd and Tb spin systems and the resulting spin dynamics about 1 ps after optical excitation. As indicated in the schematics by the thickness of the arrow and analyzed in detail below, we identify either (i) weak ($L = 0$, Gd) or (ii) strong ($L = 3$, Tb) coupling of the 4f spins to the phonon heat bath with transient temperature T_{ph}. While in (i) the 4f spins (blue arrows) remain cold and aligned along the magnetization direction M_z, in (ii), they become strongly excited by the hot phonons and thereby tilted with respect to M_z (yellow arrows). The 5d spins (red arrows) are additionally excited by coupling to the hot valence electrons T_{el} and either (i) quiver around the cold 4f spins or (ii) parallel more the dynamics of the excited 4f spins due to the intra-atomic exchange interaction.

Here, we establish ultrafast demagnetization by generation of spin excitations via direct coupling between lattice motion and 4f magnetic moments. To this end, we recorded for ferromagnetic Tb metal in parallel the exchange splitting of the 5d valence band and the 4f magnetic linear dichroism (MLD) in a time-resolved photoemission experiment. Thereby, we show that the Tb 4f spin system demagnetizes with a time constant of only 400 fs. Orbital-resolved spin dynamics simulations and the comparison to Gd corroborate that this ultrafast decay is driven by the coupling between 4f spin and phonon subsystems. Intra-atomic exchange couples excited 5d to 4f spins. Therefore, Tb 5d6s magnetic moment and the valence band exchange splitting parallel the ultrafast 4f dynamics, revealing comparable magnetization decay constants. Our results establish the coupling between lattice excitations and spin system as a mechanism that can drive ultrafast magnetization dynamics particularly in materials with strong spin-orbit coupling and concomitant large magnetic anisotropy.

RESULTS

Figure 2 shows angle-resolved photoemission spectra (ARPES) of Tb for two opposite in-plane magnetization directions $\vec{M}$ (red and blue lines) recorded with a photon energy of 40.0 eV. We use the MLD in ARPES, which is a magnetic effect comparable to the transversal magneto-optical Kerr effect in a photon-in/photon-out experiment, and directly proportional to the ferromagnetic magnetization. As shown in the inset, a chiral geometry $[\vec{E} \cdot (\vec{M} \times \vec{k}) \neq 0]$ was chosen to measure the 4f MLD in normal emission ($\vartheta = 0^\circ$) (*20*). Both the 4f high-spin final state $^8S_{7/2}$ at 2.5-eV binding energy and the low-spin multiplet components at 7.5 eV show pronounced intensity differences for opposite magnetization directions. Likewise, a small MLD is present in the $5d_{z^2}$ surface state. The MLD signal (gray backfilled area) is obtained by integration over the absolute value of the difference of blue and red spectra. In thermal equilibrium, it is proportional to the sample magnetization, and we assume that this holds for laser excitation. The single high-spin $^8S_{7/2}$ final state component at 2.5-eV binding energy shows remarkably strong dichroism. The spin multiplet at 7.5 eV consists of three components ^6D, ^6I, and ^6P, where ^6I dominates at the used photon energy. All components undergo a surface-core-level shift of ~0.26 eV (*20*). A complete set of time-resolved photoemission spectra is shown in fig. S1. Comparing the MLD of the low- and high-spin components, we find no significant difference (see the Supplementary Materials and fig. S3). Therefore, we evaluated the intense $^8S_{7/2}$ high-spin final state to follow the time evolution of the 4f magnetic moment. The 5d exchange splitting was determined by

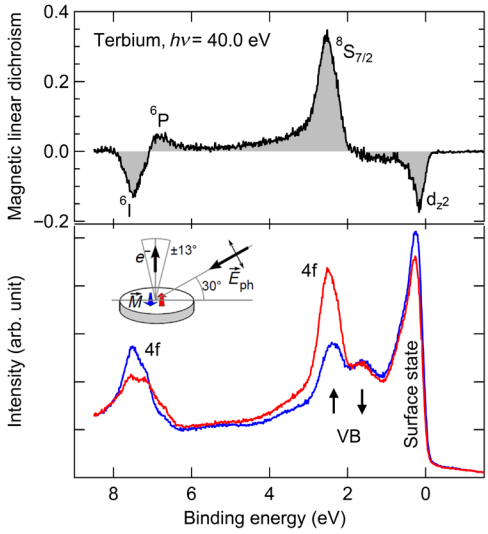

Fig. 2. Valence band photoemission spectra and MLD of Tb at 90 K. ARPES spectra probed with p-polarized light for opposite in-plane magnetization directions (red and blue, see inset) at normal emission $\vartheta = 0°$. The gray backfilled difference spectrum highlights the MLD, which was evaluated for the $^8S_{7/2}$ spin component. The binding energy of minority (↓) and majority (↑) spin 5d valence bands (VB) and the exchange splitting were extracted at $\vartheta = 8°$ (see text).

fits to the spectrum recorded at a photon energy of 36.8 eV and an emission angle of 8°, where the majority spin (↑) and minority spin (↓) branches of the valence band are energetically separated from the 4f high-spin multiplet component $^8S_{7/2}$ and do not overlap (see fig. S2) (*21*).

With the combined measurement of valence band exchange splitting and MLD, we can follow the dynamics of the 5d and 4f spins as we drive the magnetic system out of equilibrium. To explore the role of 5d-4f intra-atomic exchange coupling J_{intra} versus 4f spin to lattice coupling α_{4f}, it is of notable help to compare the spin dynamics in Tb with our previously reported results on Gd (*5*). The orbital-resolved dynamics of Gd and Tb are shown in Fig. 3 (A and B), respectively. Data (filled circles) in the upper panels correspond to the 5d exchange splitting, and data in the lower panels show the 4f MLD. Solid lines are the results from atomistic spin dynamics simulations, described below.

Optical excitation leads to a considerably stronger reduction in the 5d exchange splitting of Tb than of Gd (45% versus 15%; note the different *y* axis scaling in Fig. 3) despite the lower absorbed pump fluence (2.5 mJ/cm^2 versus 3.5 mJ/cm^2). In addition, fitting single exponentials to the ultrafast decay of the exchange splitting (see the Supplementary Materials and fig. S4), we extract clearly different time constants of about 300 fs for Tb and 700 fs for Gd. Obviously, optical excitation acts faster and more efficiently on the Tb than on the Gd 5d spin subsystem. The 5d6s valence electronic structure shows only subtle differences at the Fermi surface (*22*), and thus, we would expect comparable dynamics for Gd and Tb when neglecting the coupling to the 4f spin subsystem. Obviously, the reason lies in the different dynamics of the 4f magnetic moments. Whereas we find an ultrafast drop of the Tb 4f MLD with $\tau_{4f} \sim 400$ fs, the demagnetization of the Gd 4f spin system is characterized by a much longer time constant of ~14 ps (Fig. 3, bottom panels, data points and black lines). Note that also the Tb 4f high-spin multiplet component at 2.5 eV remains unaffected by the near-infrared (NIR) pump pulse. Bremsstrahlung isochromat spectroscopy finds the lowest lying unoccupied 4f level of Tb and of Gd out of the range of the used NIR excitation at about 2.8 and 4.5 eV above the Fermi energy, respectively (*23*).

The ab initio calculated intra-atomic exchange J_{intra} is strong for both Gd and Tb (137 and 212 meV). This would in each of the two materials translate to 5d-4f coupling times $\hbar/J_{intra}$ of below 10 fs. However, we see very different spin dynamics in the two materials. Consequently, very effective demagnetization of the Tb 4f spin system must take place via coupling to the phonons. For Tb, with its large orbital momentum *L*, the heated lattice constitutes an additional channel providing fluctuations and dissipation as well as a sink for angular momentum.

To substantiate these qualitative arguments, we analyzed the magnetization dynamics with the orbital-resolved spin model, sketched in Fig. 1 and outlined in detail in Materials and Methods and the Supplementary Materials. The stochastic Landau-Lifshitz-Gilbert (LLG) Eq. 2 describes the precessional motion of spins and its coupling to the electron and phonon subsystems via the orbital-dependent damping constants α_{5d} and α_{4f}, which are proportionality constants for how strongly the magnetic energy can be changed (see the Supplementary Materials). The 5d and 4f spin dynamics are excited by the thermal fluctuations of the electron system and the phonon heat bath, respectively. Because of the similar valence electronic structure of Gd and Tb, we necessarily assume equal damping constants $\alpha_{5d} = 0.00013$ for the itinerant 5d moments in both metals (*5*). For the 4f coupling parameter in the LLG Eq. 2, we have to use distinct values of $\alpha_{4f}^{Gd} = 0.0015$ and $\alpha_{4f}^{Tb} = 0.35$. These values of α are also consistent with magnetic resonance spectra in Gd (*24*) and Tb metal. From the ferromagnetic resonance linewidths of 5 to 10 kOe in (*25*), we deduce for Tb $\alpha = 0.1 - 0.2$.

Moreover, we find that these values yield satisfactory agreement between simulation results and the 4f MLD signal over the complete delay range, i.e., including both the (ultrafast, nonequilibrium) decay and the slow (in-equilibrium) picosecond recovery of the magnetization. In our simulation, the valence electronic subsystem is optically excited, and electron and phonon temperatures (T_{el} and T_{ph}) are calculated in an extended two-temperature model, taking spin excitations into account (see Fig. 1, the Supplementary Materials, and fig. S6) (*26*). The demagnetization of the Tb 4f moments depends on both the coupling G_{ep} between electrons and phonons and the damping α_{4f}^{Tb} between phonons and 4f moments (cf. Fig. 1). Consequently, the time constant of ultrafast demagnetization will be set by the slower process. We find that for damping constants α_{4f} larger than 0.35, the demagnetization time τ_{4f} is limited by how fast the heat flows from the electron to the phonon subsystem (see the Supplementary Materials and fig. S7).

The blue and black solid lines in the bottom panels of Fig. 3 show the calculated 5d and 4f magnetic moments as a function of pump-probe delay. Our simulations corroborate that despite large intra-atomic exchange J_{intra}, the magnetization dynamics of both metals is essentially determined by coupling of the total 4f spin subsystem to the phononic system. In Tb, strong spin-phonon coupling supports ultrafast femtosecond dynamics; in Gd, weak spin-phonon coupling leads to a slow picosecond dynamics of the 4f moment.

In contrast, the 5d magnetic moment shows an ultrafast response in both metals, because the valence-band electrons are not only coupled to the 4f system but also directly excited by the laser pulse. The fact that $\mu_{5d}^{Gd} = 0.55\ \mu_B$ is larger than $\mu_{5d}^{Tb} = 0.34\ \mu_B$ results in

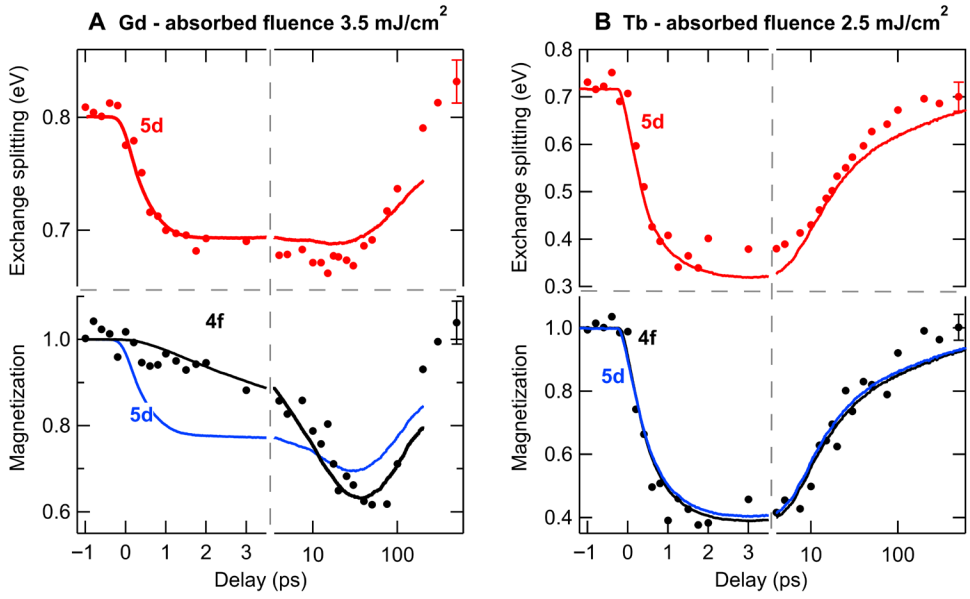

Fig. 3. Magnetization dynamics of itinerant 5d and localized 4f moments in the rare earth metals Gd and Tb. The upper panels show the response of the 5d valence band exchange splitting, and the lower panels show the transient MLD of the 4f level for (**A**) Gd and (**B**) Tb, respectively. Error bars on the last data points show 2 SDs. The solid lines result from our orbital-resolved spin dynamics simulations using ab initio input parameters for J_{ij} and J_{intra}. In the lower panels, the calculated reduced magnetization is shown. In the upper panels, the calculated dynamics of 5d magnetic moments is converted into the transient exchange splitting via first principles calculations (see the Supplementary Materials).

a shorter 5d time constant ($\propto \mu_{5d}^{-1}$, Eq. 2) in Tb as compared with Gd. In addition, the coupling to the 4f dynamics via J_{intra} affects the 5d spin dynamics. Therefore, the Tb 5d magnetic moment nearly parallels the ultrafast dynamics of the much larger 4f magnetic moment (Fig. 3A, bottom panel).

To compute the 5d exchange splitting from our spin dynamics simulation data (red solid line in Fig. 3, top panels), we determined the average angle between the 4f and 5d spin moments as a function of pump-probe delay. The noncollinear arrangement of the two on-site moments reflects the different degrees of excitation of the 5d and 4f spin subsystems. We performed ab initio calculations, which give us the electronic band structure and the exchange splitting (see the Supplementary Materials and figs. S8 and S9). The good agreement with the experimental data corroborates that the exchange splitting mainly reflects the dynamics of the 5d magnetic moment.

DISCUSSION

Our pump-probe measurements reveal a very different ultrafast demagnetization dynamics in Tb as compared with Gd. The itinerant 5d spin moment and the localized 4f moment in Tb exhibit very similar decay constants, whereas for Gd, the 5d and 4f decay constants are vastly different. This peculiar distinctive behavior between Tb and Gd allows us to pin down an essential mechanism for ultrafast magnetization dynamics that thus far has not been identified, the coupling of the 4f spin to the lattice via the orbital momentum.

This distinction between Gd and Tb is observable in several equilibrium quantities, as the mentioned 4f orbital moments of ~0 μ_B versus 3 μ_B for Gd and Tb, respectively. The coupling of the 4f moment to the lattice is reflected as well in the magnetocrystalline anisotropy energies of 0.03 meV for Gd (*27*) but 16.5 meV for Tb (*28*). In an earlier theoretical investigation, Hübner and Bennemann (*16*) concluded that the 4f spin–phonon scattering rate is related to the magnetocrystalline anisotropy energy. Therefore, the spin-lattice couplings of Gd and Tb should differ by orders of magnitude. The spin-lattice coupling furthermore determines the magnetization damping α_{4f}, which, as mentioned above, is very different for Gd and Tb. Using the very distinct values for α_{4f} in the orbital-resolved spin dynamics simulations, a very good agreement with the measurements is obtained, substantiating the important role of the 4f spin-lattice coupling identified here that leads to ultrafast excitations of magnons.

We note that a very different kind of spin-lattice coupling in the form of Elliott-Yafet electron-phonon spin-flip scattering was proposed previously as a mechanism for ultrafast demagnetization (*11*). In this mechanism, spin-polarized itinerant electrons scatter with phonons and lose angular momentum that is transferred to the lattice (*12*). A recent work suggests to have observed a corresponding rotation of the lattice (*13*). We find a different process: A fast heating of the phonon subsystem by electron-phonon scattering combined with strong coupling of the 4f orbital momentum to the lattice, in addition to the strongly coupled spin and orbital moments, drives a fast demagnetization of the Tb 4f moments via excitation of spin waves. Because of the absence of this demagnetization channel in Gd, the demagnetization dynamics has to be driven via the excited 5d moment. Despite strong intra-atomic exchange, this is less efficient because the 4f magnetic moment is large and has an intrinsically slower dynamics in the exchange field of 5d magnetic moments.

To put our work further in perspective, we compare it with other demagnetization experiments. The first experiment on Gd and Tb magnetization dynamics by Wietstruk *et al.* (*15*) probed the unoccupied 4f orbital at the M_5 edge with x-ray magnetic circular dichroism (XMCD). These measurements revealed an ultrafast demagnetization of both the Gd and Tb 4f spin systems with identical time constants of about 700 fs. A subsequent slower step exhibited

decay times of 40 and 8 ps for Gd and Tb, respectively. The difference on the slow picosecond time scale was attributed to the distinct 4f spin–lattice coupling. The identical 700-fs response constant seen for Gd and Tb in XMCD is challenged by our time-resolved photoemission experiment: Gd shows very different time scales of 5d and 4f spin dynamics with $\tau_{5d} \sim 700$ fs but $\tau_{4f} \sim 14$ ps (Fig. 3A). These order-of-magnitude-apart time constants were corroborated by a spin- and time-resolved photoemission study of the Gd surface state (*3*). The exchange splitting of bulk and Gd 5d–derived surface state show comparable ultrafast responses, but the spin polarization of the surface state is set by the 4f magnetic moment and follows the 14-ps decay seen in 4f MLD. Hence, our ARPES data for Tb show faster dynamics as compared with the XMCD measurements. We find similar decay constants of 5d exchange splitting and 4f MLD of about 300 and 400 fs (Fig. 3B).

How can we explain the different time constants seen in XMCD and ARPES? Photoelectron spectroscopy is a surface-sensitive technique probing the first few monolayers of a metal film. Thus, our photoemission data are not overlaid by spin transport across the rare-earth/tungsten interface. Currents emerging from cap layers and substrates have been proven to give sizable contributions to ultrafast magnetization dynamics (*14*, *29*–*31*). Because the XMCD experiments by Wietstruk *et al.* (*15*) probed the complete magnetic layer in transmission, they are susceptible to these spin transport contributions. Spin currents will alter the spin polarization of the 5d6s valence states. The spin polarization of the surface state is set by the 4f moment (*3*). By analogy, spin currents can in turn affect the 4f spin dynamics.

In contrast, indirect excitation of the 4f spin subsystem via intra-atomic exchange coupling to the spins of the optically excited 5d6s valence electrons results in similar responses and cannot explain the evidently different 4f spin dynamics of Tb and Gd. The 5d6s valence electronic systems of ferromagnetic Gd and Tb are very similar, and the intra-atomic exchange is qualitatively comparable and, in particular, much stronger than the 5d-5d interatomic exchange. In our simulations, we obtain qualitatively the same spin dynamics for Tb if we replace the exchange constants of Tb with those for Gd. In other words, it is not the larger intra-atomic exchange J_{intra} that drives ultrafast magnetization dynamics of the 4f spins in Tb, but the finite orbital momentum *L*. The clear difference in the magnetization dynamics of Gd and Tb must be ascribed to an additional excitation source. This is evidently the coupling to the lattice, which is weak in Gd but strong in Tb and can thus accommodate the necessary change in Tb 4f angular momentum. The different ultrafast spin dynamics in Gd and Tb are captured in Fig. 1 (A and B). In Gd, the 4f spins remain cold, and we see separate 5d spin dynamics, while in Tb, we observe ultrafast generation of coupled 5d-4f spin excitations, which can be viewed as multiple spin-wave excitations. Thus, the coupling between 4f spin and lattice excitations is crucial for ultrafast spin-wave generation and magnetization dynamics in anisotropic rare-earth metals.

In summary, time- and angle-resolved photoelectron spectroscopy with pulsed extreme ultraviolet light from higher-order harmonic generation (HHG) recording both the valence band exchange splitting and the 4f MLD allows us to unravel the fundamentally different spin dynamics of Tb and Gd due to distinct couplings of 5d and 4f spin systems to electron and lattice excitations. In Tb, thermally driven lattice fluctuations effectively couple to the 4f spin system. In Gd, the weak influence of phonons on the 4f magnetic ordering hampers this process, which explains why the ultrafast demagnetization, i.e., the subpicosecond decay of the 4f moment, is much larger in Tb than in Gd. The Tb 4f demagnetization occurs on a time scale of 400 fs. This establishes spin-lattice coupling mediated by the orbital momentum as a new mechanism that can drive ultrafast magnetization dynamics by generation of spin waves. The ferromagnetic rare-earth metals Gd and Tb have been shown to be of particular interest, since in ferrimagnetic-ordered systems, the interplay between faster 3d and slower 4f spin dynamics is seen as the origin of helicity-independent all-optical switching (*2*, *9*), and single-shot switching is so far a peculiarity of 3d-4f compounds containing Gd or Tb (*2*, *8*–*10*, *32*). Our results suggest that lattice interactions are a decisive ingredient as well to the microscopic understanding of all-optical switching.

MATERIALS AND METHODS

Experimental setup

The ARPES experiment combines an HHG beamline with an ultrahigh-vacuum endstation (*33*, *34*). We used the NIR laser fundamental ($\hbar\omega = 1.60$ eV) as pump pulse and its 23rd or 25th harmonics as probe pulse ($\hbar\omega = 36.8$ or 40.0 eV). The cross correlation of pump and probe pulses was below 120 fs. The laser operates at a repetition rate of 10 kHz. Photoelectrons were detected downstream of a hemispherical analyzer separating in parallel kinetic energy and polar emission angle within an acceptance range of 9 eV and ±13°, respectively. The combined energy resolution of HHG source and electron detector was 0.2 eV.

Sample preparation

Tb films of 10-nm thickness were prepared by molecular beam epitaxy on the (110) surface of a tungsten single crystal at a pressure of 1×10^{-10} mbar. After annealing for 1 min at 880 K, the film showed the sharp low-energy electron diffraction (LEED) pattern of the (0001) surface of hexagonal close packed (hcp) Tb. Substrate and thin film quality were controlled by LEED and ARPES (*35*) (see the "Sample quality" section of the Supplementary Materials for further details).

Orbital-resolved spin dynamics simulation

For the theoretical description of the ultrafast demagnetization, we adopted the orbital-resolved spin model sketched in Fig. 1 (*5*, *9*). We distinguish localized 4f moments with $\mu_{4f}^{Tb} = 9\,\mu_B$, which contain both spin and orbital moments and itinerant 5d spin moments with $\mu_{5d}^{Tb} = 0.34\,\mu_B$ (*36*). We treat the Tb 4f moment as a single effective spin μ_{4f}^{Tb}. The NIR pump laser excites the 5d valence electrons but cannot directly excite the 4f electrons. Energy will thus flow from the heated electrons to the lattice via electron-phonon coupling G_{ep} as well as to the 5d spin system α_{5d} (yellow arrows in Fig. 1). The large Tb 4f orbital moment strongly couples to the lattice because of the strong spin-orbit energy, and the Tb spin and orbital momenta are tightly bound. This chain of interactions results in a large spin-to-lattice coupling. In addition, the 4f moments can be excited via the strong intra-atomic exchange interaction to the laser-excited 5d spins. Introducing the normalized moments $\mathbf{S_i} = \mu_i/\mu$, at lattice site *i*, the full orbital-resolved spin Hamiltonian can be written as

$$\begin{aligned}\mathcal{H} = &-\sum_{i,j} J_{ij}\,\mathbf{S}_i^{5d}\cdot\mathbf{S}_j^{5d} - J_{\mathrm{intra}}\sum_i \mathbf{S}_i^{5d}\cdot\mathbf{S}_i^{4f} \\ &- d_2\sum_i \cos^2\vartheta_i^{4f} - d_6^6\sum_i \sin^6\vartheta_i^{4f}\cos 6\varphi_i^{4f}\end{aligned} \tag{1}$$

We calculated the inter- and intra-atomic exchange interactions by first principles methods and validated J_{ij} and J_{intra} by the temperature dependence of the magnetization (see the Supplementary Materials and fig. S10). Higher terms in Eq. 1 describe the Tb-specific uniaxial and basal plane magnetocrystalline anisotropy ($d_{2,\text{Tb}} = -16.5$ meV and $d^{6}_{6,\text{Tb}} = 48$ μeV) (*28*). To compute the spin dynamics, we numerically solve the stochastic LLG equation for both orbitals ν as shown in (*5*)

$$\frac{\partial \mathbf{S}_i^{\nu}}{\partial t} = \frac{-\gamma_{\nu}}{(1+\alpha_{\nu}^2)\mu_{\nu}} \mathbf{S}_i^{\nu} \times (\mathbf{H}_i^{\nu} + \alpha_{\nu} \mathbf{S}_i^{\nu} \times \mathbf{H}_i^{\nu}) \quad (2)$$

The Tb gyromagnetic ratios are $\gamma_{5d} = 2\ \mu_B/\hbar$ and $\gamma_{5d} = 1.5\ \mu_B/\hbar$, and the orbital-dependent Gilbert dampings are α_v. The effective field that enters the LLG equation is given by

$$\mathbf{H}_i^{\nu} = -\frac{\partial \mathcal{H}}{\partial \mathbf{S}_i^{\nu}} + \zeta_i^{\nu} \quad (3)$$

where ζ_i^{ν} represents thermal fluctuations in the form of Gaussian white noise proportional to the transient electron and lattice temperatures for the cases of 5d and 4f moments, respectively (*5*). The temperatures of the electron and phonon subsystems are computed with an extended two-temperature model (*26*, *37*) [for parameters, see (*5*, *38*)].

Tb exchange constants and exchange splitting

The present ab initio calculations of the interatomic exchange constants in Tb are based on the tight-binding linear muffin-tin orbital method (*39*) using the atomic-sphere approximation (ASA). The Vosko-Wilk-Nursair exchange potential has been used within the local spin-density approximation (*40*). As the 4f electrons do not take part in the interatomic exchange, they were included as core electrons in this calculation. The intra-atomic exchange and the 5d exchange splitting, conversely, do depend sensitively on the correlated 4f states. We computed these quantities using the LSDA+*U* approach (*41*) within a full-potential electronic structure program with spin-orbit coupling included. The magnetic interactions were mapped onto the effective Heisenberg Hamiltonian of Eq. 1. Exchange interactions between different sites, J_{ij} (see fig. S10A), were calculated using the magnetic force theorem (*42*).

The complex nonequilibrium situation with the 4f magnetization at an elevated temperature, and the 5d spin subsystem at a different temperature, leads to their noncollinear alignment. The exchange splitting depends on the magnetic disorder of the 4f moments and, in addition, on the average relative angle θ between $\mathbf{S}^{5d}$ and $\mathbf{S}^{4f}$. To evaluate this dependence, we use an ab initio description based on the linear plane wave method (see the "Tb density of states" section of the Supplementary Materials), while the directions of the spd magnetic moments are constrained (*5*) so that their angle with respect to (w.r.t.) the 4f momentum direction is θ. For this constrained system, we calculate the resulting band structure and extract the exchange splitting of the valence bands at the Γ point. For further details, see the "5d exchange-splitting" section of the Supplementary Materials.

The Supplementary Materials for further details on ab initio calculations, spin dynamics simulations, and the evaluation of the angle-resolved photoemission data accompany this paper at http://www.scienceadvances.org/.

SUPPLEMENTARY MATERIALS

Supplementary material for this article is available at http://advances.sciencemag.org/cgi/content/full/6/39/eabb1601/DC1

REFERENCES AND NOTES

1. E. Beaurepaire, J.-C. Merle, A. Daunois, J.-Y. Bigot, Ultrafast spin dynamics in ferromagnetic nickel. *Phys. Rev. Lett.* **76**, 4250–4253 (1996).
2. I. Radu, K. Vahaplar, C. Stamm, T. Kachel, N. Pontius, H. A. Dürr, T. A. Ostler, J. Barker, R. F. L. Evans, R. W. Chantrell, A. Tsukamoto, A. Itoh, A. Kirilyuk, T. Rasing, A. V. Kimel, Transient ferromagnetic-like state mediating ultrafast reversal of antiferromagnetically coupled spins. *Nature* **472**, 205–208 (2011).
3. B. Andres, M. Christ, C. Gahl, M. Wietstruk, M. Weinelt, J. Kirschner, Separating exchange splitting from spin mixing in gadolinium by femtosecond laser excitation. *Phys. Rev. Lett.* **115**, 207404 (2015).
4. P. Tengdin, W. You, C. Chen, X. Shi, D. Zusin, Y. Zhang, C. Gentry, A. Blonsky, M. Keller, P. M. Oppeneer, H. C. Kapteyn, Z. Tao, M. M. Murnane, Critical behavior within 20 fs drives the out-of-equilibrium laser-induced magnetic phase transition in nickel. *Sci. Adv.* **4**, eaap9744 (2018).
5. B. Frietsch, J. Bowlan, R. Carley, M. Teichmann, S. Wienholdt, D. Hinzke, U. Nowak, K. Carva, P. M. Oppeneer, M. Weinelt, Disparate ultrafast dynamics of itinerant and localized magnetic moments in gadolinium metal. *Nat. Commun.* **6**, 8262 (2015).
6. R. Carley, K. Döbrich, B. Frietsch, C. Gahl, M. Teichmann, O. Schwarzkopf, P. Wernet, M. Weinelt, Femtosecond laser excitation drives ferromagnetic gadolinium out of magnetic equilibrium. *Phys. Rev. Lett.* **109**, 057401 (2012).
7. S. Eich, M. Plötzing, M. Rollinger, S. Emmerich, R. Adam, C. Chen, H. C. Kapteyn, M. M. Murnane, L. Plucinski, D. Steil, B. Stadtmüller, M. Cinchetti, M. Aeschlimann, C. M. Schneider, S. Mathias, Band structure evolution during the ultrafast ferromagnetic-paramagnetic phase transition in cobalt. *Sci. Adv.* **3**, e1602094 (2017).
8. C. D. Stanciu, F. Hansteen, A. V. Kimel, A. Kirilyuk, A. Tsukamoto, A. Itoh, T. Rasing, All-optical magnetic recording with circularly polarized light. *Phys. Rev. Lett.* **99**, 047601 (2007).
9. S. Wienholdt, D. Hinzke, K. Carva, P. M. Oppeneer, U. Nowak, Orbital-resolved spin model for thermal magnetization switching in rare-earth-based ferrimagnets. *Phys. Rev. B* **88**, 020406(R) (2013).
10. M. L. M. Lalieu, M. J. G. Peeters, S. R. R. Haenen, R. Lavrijsen, B. Koopmans, Deterministic all-optical switching of synthetic ferrimagnets using single femtosecond laser pulses. *Phys. Rev. B* **96**, 220411(R) (2017).
11. B. Koopmans, G. Malinowski, F. Dalla Longa, D. Steiauf, M. Fähnle, T. Roth, M. Cinchetti, M. Aeschlimann, Explaining the paradoxical diversity of ultrafast laser-induced demagnetization. *Nat. Mater.* **9**, 259–265 (2010).
12. K. Carva, M. Battiato, P. M. Oppeneer, Ab initio investigation of the Elliott-Yafet electron-phonon mechanism in laser-induced ultrafast demagnetization. *Phys. Rev. Lett.* **107**, 207201 (2011).
13. C. Dornes, Y. Acremann, M. Savoini, M. Kubli, M. J. Neugebauer, E. Abreu, L. Huber, G. Lantz, C. A. F. Vaz, H. Lemke, E. M. Bothschafter, M. Porer, V. Esposito, L. Rettig, M. Buzzi, A. Alberca, Y. W. Windsor, P. Beaud, U. Staub, D. Zhu, S. Song, J. M. Glownia, S. L. Johnson, The ultrafast Einstein-de Haas effect. *Nature* **565**, 209–212 (2019).
14. M. Battiato, K. Carva, P. M. Oppeneer, Superdiffusive spin transport as a mechanism of ultrafast demagnetization. *Phys. Rev. Lett.* **105**, 027203 (2010).
15. M. Wietstruk, A. Melnikov, C. Stamm, T. Kachel, N. Pontius, M. Sultan, C. Gahl, M. Weinelt, H. A. Dürr, U. Bovensiepen, Hot-electron-driven enhancement of spin-lattice coupling in Gd and Tb 4*f* ferromagnets observed by femtosecond X-ray magnetic circular dichroism. *Phys. Rev. Lett.* **106**, 127401 (2011).
16. W. Hübner, K. H. Bennemann, Simple theory for spin-lattice relaxation in metallic rare-earth ferromagnets. *Phys. Rev. B* **53**, 3422–3427 (1996).
17. A. Melnikov, A. Povolotskiy, U. Bovensiepen, Magnon-enhanced phonon damping at Gd(0001) and Tb(0001) surfaces using femtosecond time-resolved optical second-harmonic generation. *Phys. Rev. Lett.* **100**, 247401 (2008).
18. A. Vaterlaus, T. Beutler, F. Meier, Spin-lattice relaxation time of ferromagnetic gadolinium determined with time-resolved spin-polarized photoemission. *Phys. Rev. Lett.* **67**, 3314–3317 (1991).
19. J. Jensen, A. R. Mackintosh, *Rare Earth Magnetism: Structures and Excitations* (Clarendon Press, Oxford, 1991).
20. K. Starke, Magnetic dichroism in core-level photoemission, in *Springer Tracts in Modern Physics*, Y. Chen, A. Fujimori, W. C. Stwalley, J. Yang, Eds. (Springer-Verlag, Berlin-Heidelberg, 2000), vol. 159.
21. M. Teichmann, B. Frietsch, K. Döbrich, R. Carley, M. Weinelt, Transient band structures in the ultrafast demagnetization of ferromagnetic gadolinium and terbium. *Phys. Rev. B* **91**, 014425 (2015).

22. K. M. Döbrich, A. Bostwick, J. L. McChesney, K. Rossnagel, E. Rotenberg, G. Kaindl, Fermi-surface topology and helical antiferromagnetism in heavy lanthanide metals. *Phys. Rev. Lett.* **104**, 246401 (2010).
23. J. K. Lang, Y. Baer, P. A. Cox, Study of the 4f and valence band density of states in rare-earth metals. II. Experiment and results. *J. Phys. F Metal Phys.* **11**, 121–138 (1981).
24. W. Platow, A. N. Anisimov, G. L. Dunifer, M. Farle, K. Baberschke, Correlations between ferromagnetic-resonance linewidths and sample quality in the study of metallic ultrathin films. *Phys. Rev. B* **58**, 5611–5621 (1998).
25. J. L. Stanford, R. C. Young, Magnetic resonance in single-crystal terbium metal at 100 GHz. *Phys. Rev.* **157**, 245–251 (1967).
26. S. I. Anisimov, B. L. Kapeliovich, T. L. Perel'man, Electron emission from metal surfaces exposed to ultrashort laser pulses. *Sov. Phys.-JETP* **39**, 375–377 (1974).
27. S. Abdelouahed, M. Alouani, Magnetic anisotropy in Gd, GdN, and $GdFe_2$ tuned by the energy of gadolinium *4f* states. *Phys. Rev. B* **79**, 054406 (2009).
28. J. J. Rhyne, A. E. Clark, Magnetic anisotropy of terbium and dysprosium. *J. Appl. Phys.* **38**, 1379–1380 (1967).
29. D. Rudolf, C. La-O-Vorakiat, M. Battiato, R. Adam, J. M. Shaw, E. Turgut, P. Maldonado, S. Mathias, P. Grychtol, H. T. Nembach, T. J. Silva, M. Aeschlimann, H. C. Kapteyn, M. M. Murnane, C. M. Schneider, P. M. Oppeneer, Ultrafast magnetization enhancement in metallic multilayers driven by superdiffusive spin current. *Nat. Commun.* **3**, 1037 (2012).
30. C. E. Graves, A. H. Reid, T. Wang, B. Wu, S. de Jong, K. Vahaplar, I. Radu, D. P. Bernstein, M. Messerschmidt, L. Müller, R. Coffee, M. Bionta, S. W. Epp, R. Hartmann, N. Kimmel, G. Hauser, A. Hartmann, P. Holl, H. Gorke, J. H. Mentink, A. Tsukamoto, A. Fognini, J. J. Turner, W. F. Schlotter, D. Rolles, H. Soltau, L. Strüder, Y. Acremann, A. V. Kimel, A. Kirilyuk, T. Rasing, J. Stöhr, A. O. Scherz, H. A. Dürr, Nanoscale spin reversal by non-local angular momentum transfer following ultrafast laser excitation in ferrimagnetic GdFeCo. *Nat. Mater.* **12**, 293–298 (2013).
31. J. Wieczorek, A. Eschenlohr, B. Weidtmann, M. Rösner, N. Bergeard, A. Tarasevitch, T. O. Wehling, U. Bovensiepen, Separation of ultrafast spin currents and spin-flip scattering in Co/Cu(001) driven by femtosecond laser excitation employing the complex magneto-optical Kerr effect. *Phys. Rev. B* **92**, 174410 (2015).
32. J. Gorchon, C.-H. Lambert, Y. Yang, A. Pattabi, R. B. Wilson, S. Salahuddin, J. Bokor, Single shot ultrafast all optical magnetization switching of ferromagnetic Co/Pt multilayers. *Appl. Phys. Lett.* **111**, 042401 (2017).
33. B. Frietsch, R. Carley, K. Döbrich, C. Gahl, M. Teichmann, O. Schwarzkopf, P. Wernet, M. Weinelt, A high-order harmonic generation apparatus for time- and angle-resolved photoelectron spectroscopy. *Rev. Sci. Instrum.* **84**, 075106 (2013).
34. B. Frietsch, PhD thesis, FU Berlin (2015); https://refubium.fu-berlin.de/handle/fub188/4663.
35. J. Zhang, P. A. Dowben, D. Li, M. Onellion, Angle-resolved photoemission study of oxygen chemisorption on Gd(0001). *Surf. Sci.* **329**, 177–183 (1995).
36. W. C. Koehler, Magnetic properties of rare-earth metals and alloys. *J. Appl. Phys.* **36**, 1078–1087 (1965).
37. M. P. Magiera, L. Brendel, D. E. Wolf, U. Nowak, Spin excitations in a monolayer scanned by a magnetic tip. *EPL (Europhys. Lett.)* **87**, 26002 (2009).
38. B. Fu, W. Lai, Y. Yuan, H. Xu, W. Liu, Calculation and analysis of lattice thermal conductivity in tungsten by molecular dynamics. *J. Nucl. Mater.* **427**, 268–273 (2012).
39. H. L. Skriver, *The LMTO Method: Muffin-Tin Orbitals and Electronic Structure* (Springer-Verlag, Berlin, 1984).
40. S. H. Vosko, L. Wilk, M. Nusair, Accurate spin-dependent electron liquid correlation energies for local spin density calculations: A critical analysis. *Can. J. Phys.* **58**, 1200–1211 (1980).
41. V. I. Anisimov, J. Zaanen, O. K. Andersen, Band theory and Mott insulators: Hubbard U instead of stoner I. *Phys. Rev. B* **44**, 943–954 (1991).
42. A. I. Liechtenstein, M. I. Katsnelson, V. A. Gubanov, Exchange interactions and spin-wave stiffness in ferromagnetic metals. *J. Phys. F. Metal Phys.* **14**, L125–L128 (1984).

Acknowledgments: We thank B. Andres for the valuable discussions. **Funding:** This project was supported by Deutsche Forschungsgemeinschaft and the Collaborative Research Center TRR 227 on *Ultrafast Spin Dynamics*, project A1. A.D. and U.N. would like to acknowledge financial support from the Center for Applied Photonics at the University of Konstanz. J.B. is indebted to the Alexander von Humboldt foundation for financial support. D.L. acknowledges support by the European Regional Development Fund in the IT4Innovations National Supercomputing Center—Path to Exascale project, project no. CZ.02.1.01/0.0/0.0/16_013/0001791 within the Operational Programme Research, Development, and Education. K.C. acknowledges support from the Czech Science Foundation (grant no. 18-07172S). P.M.O. acknowledges support by the Swedish Research Council (VR), the K. and A. Wallenberg Foundation (contract no. 2015.0060), and the EU H2020 Research and Innovation Programme (grant no. 737709). **Author contributions:** The design of the study was carried out by K.D. and M.W. The realization of the high-order harmonics experiment was carried out by B.F., R.C., M.T., K.D., and M.W. Data were collected by B.F., R.C., and J.B. Experimental data analysis was carried out by B.F. with input from all authors. Ab initio calculations were performed by K.C., D.L., and P.M.O. Atomistic spin dynamics simulations were carried out by A.D. and U.N. The manuscript was prepared by M.W., A.D., and P.M.O. with input from all authors. **Competing interests:** The authors declare that they have no competing interests. **Data and materials availability:** All data needed to evaluate the conclusions in the paper are present in the paper and/or the Supplementary Materials. Additional data related to this paper may be requested from the authors.

Submitted 4 February 2020
Accepted 25 June 2020
Published 23 September 2020
10.1126/sciadv.abb1601

Citation: B. Frietsch, A. Donges, R. Carley, M. Teichmann, J. Bowlan, K. Döbrich, K. Carva, D. Legut, P. M. Oppeneer, U. Nowak, M. Weinelt, The role of ultrafast magnon generation in the magnetization dynamics of rare-earth metals. *Sci. Adv.* **6**, eabb1601 (2020).